

DOPPLER MONITORING OF THE WASP-47 MULTIPLANET SYSTEM*

FEI DAI¹, JOSHUA N. WINN¹, PAMELA ARRIAGADA², R. PAUL BUTLER², JEFFREY D. CRANE³, JOHN ASHER JOHNSON⁴,
STEPHEN A. SHECTMAN³, JOHANNA K. TESKE^{2,3}, IAN B. THOMPSON³, ANDREW VANDERBURG⁴, ROBERT A. WITTENMYER^{5,6}

Draft version October 30, 2015

ABSTRACT

We present precise Doppler observations of WASP-47, a transiting planetary system featuring a hot Jupiter with both inner and outer planetary companions. This system has an unusual architecture and also provides a rare opportunity to measure planet masses in two different ways: the Doppler method, and the analysis of transit-timing variations (TTV). Based on the new Doppler data, obtained with the Planet Finder Spectrograph on the Magellan/Clay 6.5m telescope, the mass of the hot Jupiter is $370 \pm 29 M_{\oplus}$. This is consistent with the previous Doppler determination as well as the TTV determination. For the inner planet WASP-47e, the Doppler data lead to a mass of $12.2 \pm 3.7 M_{\oplus}$, in agreement with the TTV-based upper limit of $< 22 M_{\oplus}$ (95% confidence). For the outer planet WASP-47d, the Doppler mass constraint of $10.4 \pm 8.4 M_{\oplus}$ is consistent with the TTV-based measurement of $15.2^{+6.7}_{-7.6} M_{\oplus}$.

Subject headings: planetary systems - planets and satellites: composition - stars: individual (WASP-47) - techniques: radial velocities

1. INTRODUCTION

The first two things one wants to know about any newly discovered planet are its mass and radius. Is it relatively small and dense, similar to Earth? Is it large and diffuse, similar to Jupiter and Saturn? Or is it somewhere in between? Although the *Kepler* mission revolutionized exoplanetary science, for the specific purpose of measuring planet masses the original mission was not ideal. This is because the typical target stars were relatively faint ($V = 14-16$), frustrating efforts to obtain high-resolution spectra that are necessary to measure planetary masses by the Doppler method. For planets smaller than Neptune, it has only been possible to measure the masses of a few dozen *Kepler* planets with the brightest host stars (Marcy et al. 2014; Howard et al. 2013; Pepe et al. 2013; Dressing et al. 2015), and even in those cases many of the mass measurements have large uncertainties.

Because of a mechanical failure and reduction in capability, the *Kepler* telescope abandoned its original mission and is now engaged in a new mission called *K2* (Howell et al. 2014). Every 3 months, the telescope observes a different field on the ecliptic (the only zone where it can achieve stable pointing), providing a fresh sample of bright stars for which precise Doppler observations are possible. The third *K2* field happened to encompass WASP-47, a G9 star with a previously discovered transiting hot Jupiter (Hellier et al. 2012). The *K2* data have revealed two additional transiting planets, with periods of 0.8 days and 9 days (Becker et al. 2015). Furthermore,

Neveu-VanMalle et al. (2015) recently reported the Doppler discovery of a second, wide-orbiting Jovian planet, with a period of 572 ± 7 days.

With this discovery, WASP-47 is unique among the known exoplanetary systems: a hot Jupiter with very close companions on both interior and exterior orbits, in addition to a distant companion. The close companions have implications for theories of hot Jupiter formation. It seems difficult to attain such a compact and fragile configuration within violent scenarios such as planet-planet scattering (Rasio & Ford 1996; Weidenschilling & Marzari 1996) or Kozai-Lidov oscillations (Mazeh et al. 1997; Holman et al. 1997; Innanen et al. 1997). The WASP-47 system also presents a rare opportunity to measure the masses of the inner three planets using two independent techniques: the traditional Doppler method, and the analysis of transit-timing variations (TTV, Holman & Murray 2005; Agol et al. 2005). It is always useful to have independent methods for measuring important quantities, and for planet masses in particular, there is some controversy over the reliability of TTV-based masses. The TTV method has revealed some planets with surprisingly low densities (see, e.g., Lissauer et al. 2013; Schmitt et al. 2014; Jontof-Hutter et al. 2014, 2015). Among the sample of planets smaller than $4.0 R_{\oplus}$, those for which masses have been determined with TTVs have systematically lower masses than the subsample for which masses have been determined with the Doppler method (Weiss & Marcy 2014). This discrepancy could be due to systematic errors in one or both methods, along with biases in the various samples. To disentangle these effects, it is useful to identify individual systems for which the Doppler and TTV methods can both be applied.

WASP-47 is precisely such an example. Becker et al. (2015) have already performed a TTV analysis of the available *K2* data for WASP-47. In this Letter we present new Doppler observations that have led to complementary mass determinations. The new data are described in Section 2, our analysis is presented in Section 3, and the implications are discussed in Section 4.

* This paper includes data gathered with the 6.5 meter Magellan Telescopes located at Las Campanas Observatory, Chile.

¹ Department of Physics and Kavli Institute for Astrophysics and Space Research, Massachusetts Institute of Technology, Cambridge, MA 02139, USA fd284@mit.edu

² Carnegie Institution of Washington, Department of Terrestrial Magnetism, 5241 Broad Branch Road, NW, Washington DC, 20015-1305, USA

³ The Observatories of the Carnegie Institution of Washington, 813 Santa Barbara Street, Pasadena, CA 91101, USA

⁴ Harvard-Smithsonian Center for Astrophysics, 60 Garden Street, Cambridge, MA 02138, USA

⁵ Exoplanetary Science at UNSW, School of Physics, UNSW Australia, Sydney, NSW 2052, Australia

⁶ Australian Centre for Astrobiology, UNSW Australia, Sydney, NSW 2052, Australia

TABLE 1
KEY PARAMETERS OF THE WASP-47 SYSTEM

Parameter	Value and 68.3% Conf. Limits	Ref.
WASP-47b		
Orbital period [days]	4.1591282 ± 0.0000046	A
Transit epoch [BJD]	$2457007.932132 \pm 0.000061$	A
Radius [R_{\oplus}]	12.71 ± 0.44	A
RV semi-amplitude K [m s^{-1}]	143.3 ± 2.5	B
RV-based mass [M_{\oplus}]	370 ± 29	B
TTV-based mass [M_{\oplus}]	341^{+73}_{-55}	A
Mean density (RV-based) [g cm^{-3}]	0.99 ± 0.13	A, B
WASP-47e		
Orbital period [days]	0.789593 ± 0.000012	A
Transit epoch [BJD]	$2457011.34859 \pm 0.00031$	A
Radius [R_{\oplus}]	1.817 ± 0.065	A
RV semi-amplitude K [m s^{-1}]	8.2 ± 2.4	B
RV-based mass [M_{\oplus}]	12.2 ± 3.7	B
TTV-based mass [M_{\oplus}]	< 22 (95% Confidence)	A
Mean density (RV-based) [g cm^{-3}]	11.2 ± 3.6	A, B
WASP-47d		
Orbital period [days]	9.03079 ± 0.00017	A
Transit epoch [BJD]	$2457006.36922 \pm 0.00052$	A
Radius [R_{\oplus}]	3.60 ± 0.13	A
RV semi-amplitude K [m s^{-1}]	3.1 ± 2.5	B
RV-based mass [M_{\oplus}]	10.4 ± 8.4	B
TTV-based mass [M_{\oplus}]	$15.2^{+6.7}_{-7.6}$	A
Mean density (RV-based) [g cm^{-3}]	1.2 ± 1.0	A, B

NOTE. — A: Becker et al. (2015); B: This work.

TABLE 2
RELATIVE RADIAL VELOCITY OF WASP-47

BJD	RV [m s^{-1}]	Unc. [m s^{-1}]
2457257.721181	-70.6	2.5
2457257.751794	-77.9	2.7
2457257.783981	-91.4	2.8
2457257.821563	-97.1	2.9
2457258.718380	-162.9	3.4
2457258.790174	-154.4	2.7
2457258.857569	-132.2	3.5
2457261.736597	-49.8	2.7
2457261.767025	-56.8	3.4
2457261.821400	-61.7	4.0
2457264.621262	130.9	3.1
2457264.722280	137.2	3.3
2457264.762627	135.0	3.9
2457264.792650	137.5	3.9
2457267.665532	-56.2	2.8
2457267.718310	-32.4	2.7
2457267.771910	-42.8	2.7
2457267.816458	-18.3	3.4
2457268.571817	112.6	3.3
2457268.673646	118.0	3.1
2457268.760174	122.2	3.4
2457268.798935	113.0	3.9
2457269.608519	39.0	2.8
2457269.710486	27.7	3.1
2457269.747708	27.7	2.7
2457269.793981	3.4	3.7

2. OBSERVATIONS

WASP-47 was observed from August 23rd to September 4th 2015 UT with the Carnegie Planet Finder Spectrograph (PFS, Crane et al. 2010) on the 6.5 meter Magellan/Clay Telescope at Las Campanas Observatory in Chile. We obtained several spectra of WASP-47 on each clear night, for a total of 27 spectra. We employed an iodine gas cell to superimpose well-characterized absorption features onto the stellar spectrum, helping to establish the wavelength scale and instrumental profile. The detector was read out in the 2×2 binned mode, to reduce readout noise. The typical exposure time was about 20 minutes, giving a signal-to-noise ratio of $\approx 73 \text{ pixel}^{-1}$ and a resolution of about 76000 in the vicinity of the iodine absorption lines. An additional spectrum with higher resolution and signal-to-noise ratio was obtained without the iodine cell, to serve as a template spectrum for the Doppler analysis.

The relative radial velocities were extracted from the spectrum using the techniques of Butler et al. (1996). The internal measurement uncertainties (ranging from $2.5\text{--}4 \text{ m s}^{-1}$) were estimated from the scatter in the results to fitting individual 2 \AA sections of the spectrum. Table 2 gives the radial velocities and the internal measurement uncertainties. Figure 1 shows the observed radial velocities.

3. ANALYSIS

We will refer to the WASP-47 planets as follows: planet b is the transiting hot Jupiter; planet c is the long-period Jupiter identified by Neveu-VanMalle et al. (2015); planet d is the transiting planet with period 9.0 days and planet e is the transiting planet with period 0.8 days.

Before modeling the Doppler data, an important question is whether it suffices to model the stellar motion as the superposition of non-interacting orbits, or whether the gravitational interactions between planets need be taken into account (which requires far more computation time). We concluded that gravitational interactions could be neglected for present purposes, based on the following test. First, we fitted the data with a model consisting of four non-interacting Keplerian orbits. Then, we took the best-fitting model parameters as the starting conditions for a dynamical five-body integration of Newton's equations of motion, using the 4th order Hermite scheme that is available on the *Systemic* console (Meschiari et al. 2009). We examined the deviations between the RVs calculated in the dynamical model and the RVs in the non-interacting model. Over the relatively short timespan of our PFS observations, the maximum deviation is only 0.14 m s^{-1} , which is much smaller than the uncertainties in the RV data and the uncertainties in the amplitudes of the Doppler signals.

We assumed the orbits of the inner three planets to be circular because tidal circularization timescales are expected to be short, at least for the two inner planets. Furthermore, Becker et al. (2015) showed that low eccentricities ($e < 0.05$) are required for all three planets in order to ensure long-term dynamical stability of the system. And from a practical point of view, with only 26 data points and relatively small Doppler amplitudes, we can gain little empirical information at this stage regarding orbital eccentricities.

Given the long period of planet c (572 ± 7 days), and the relatively short interval of our PFS observations, we do not attempt to characterize planet c. Instead, we adopted the best-fitting parameters for planet c reported by Neveu-VanMalle et al. (2015), and subtracted its expected

contribution from the Doppler data, prior to our analysis. (Although we performed this step for completeness, in practice the contribution from planet c has no substantial effect on the results.)

With these choices, our model has 5 free parameters: the semi-amplitude K of the radial-velocity variation induced by each of the 3 inner planets, an arbitrary additive constant γ (since only the relative radial velocities are measured precisely), and a “jitter” term σ_j that is added in quadrature with the internal measurement uncertainty. The jitter term is intended to account for additional sources of uncorrelated uncertainties, which could be of astrophysical or instrumental origin. We held fixed the orbital periods and transit epochs at the values reported by Becker et al. (2015), as they have negligible uncertainties for our purposes. We adopted a likelihood function

$$\mathcal{L} = \prod_{i=1}^N \left(\frac{1}{\sqrt{2\pi(\sigma_i^2 + \sigma_j^2)}} \exp \left[-\frac{[RV(t_i) - \mathcal{M}(t_i)]^2}{2(\sigma_i^2 + \sigma_j^2)} \right] \right), \quad (1)$$

where $RV(t_i)$ is the measured radial velocity at time t_i ; $\mathcal{M}(t_i)$ is the calculated radial velocity at time t_i for a particular choice of model parameters; σ_i is the internal measurement uncertainty; and σ_j is the jitter. Uniform priors were adopted for all the model parameters.

We maximized the likelihood using the Nelder-Mead (“Amoeba”) method. The best-fitting model is shown by a red line in the top panel of Figure 1. The lower panel shows the residuals. Figure 2 shows the radial-velocity variation specific to each planet, based on the data and the parameters of the best-fitting model.

To determine the parameter uncertainties and covariances we employed a Markov Chain Monte Carlo method. In particular we used the affine-invariant ensemble sampler proposed by Goodman & Weare (2010). We started 100 chains in a Gaussian “ball” in the neighborhood of the best-fitting model parameters. We stopped the chains when the Gelman-Rubin potential scale reduction factor (Gelman & Rubin 1992) dropped to 1.01, a standard criterion for adequate convergence. The posterior probabilities of all parameters are smooth and unimodal. Table 1 reports the results. The reported “best fit” value is the median of the marginalized posterior distribution. The reported uncertainty interval encompasses the range between the 16% and 84% percentile levels of the cumulative distribution. The result for the jitter parameter was $6.1^{+1.4}_{-1.1} \text{ m s}^{-1}$, about twice as large as the internal measurement uncertainty.

The motion induced by the hot Jupiter WASP-47b was clearly detected, with a semi-amplitude $K_b = 143.3 \pm 2.5 \text{ m s}^{-1}$. This result is consistent with the previously reported Doppler data of Hellier et al. (2012), who found $K_b = 136 \pm 5 \text{ m s}^{-1}$. The inner planet WASP-47e was detected at the 3.4σ level, with $K_e = 8.2 \pm 2.4 \text{ m s}^{-1}$. The motion induced by the outer planet WASP-47d was detected weakly if at all, leading to the result $K_d = 3.1 \pm 2.5 \text{ m s}^{-1}$ if we allow the semi-amplitude to range over both positive and negative numbers. If we require the semi-amplitude to be positive, we obtain an upper limit of 8.3 m s^{-1} with 95% confidence.

The root-mean-squared residual between the data and the best-fitting three-planet model was 6.08 m s^{-1} . As another measure of the significance of each planet detection, we tried refitting the data with different numbers of planets. When

only planet b is modeled (i.e., $K_c = K_d \equiv 0$) the root-mean-squared (rms) residual between the data and the best-fitting model is 9.16 m s^{-1} . When WASP-47e is included in the model, the rms residual drops to 6.34 m s^{-1} . It drops further to 6.08 m s^{-1} when all three planets are modeled.

The planetary masses can be calculated from the semi-amplitudes, orbital periods, and stellar mass. In doing so we adopted a stellar mass of $M_* = 1.04 \pm 0.08 M_\odot$ (Mortier et al. 2013). The results are given in Table 1a. This table also provides planetary mean densities, based on the masses from our work and the radii reported by Becker et al. (2015) based on the K2 transit photometry. The best-fitting model satisfies the heuristic criterion for long-term dynamical stability that was proposed by Fabrycky et al. (2014): $\Delta_{\text{in}} + \Delta_{\text{out}} > 18$, where Δ is the difference between semi-major axes of the inner and outer pairs of planets measured in terms of their mutual Hill radius.

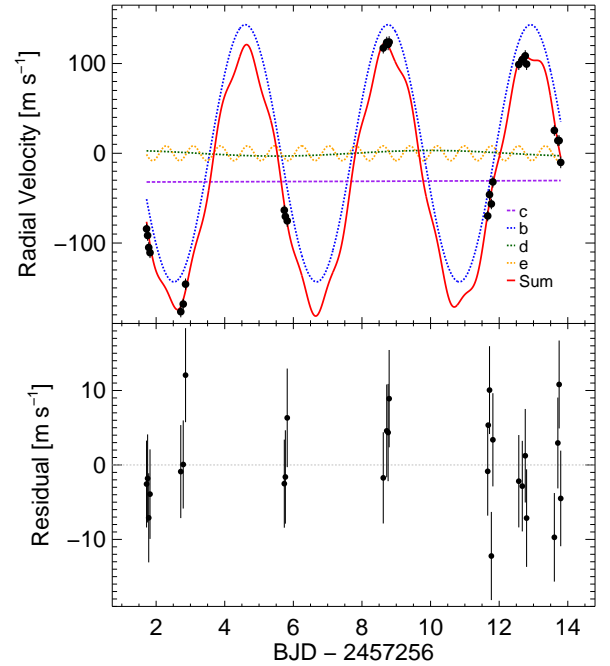


FIG. 1.— *Top*.—Measured radial velocity of WASP-47 (black dots) along with the best-fitting model (red line). The contributions to the model from each planet are also plotted as colored curves. *Bottom*.—Differences between the data and the best-fitting model. The error bars represent the quadrature sum of the internally-estimated measurement uncertainties, and the fitted jitter parameter ($6.1^{+1.4}_{-1.1} \text{ m s}^{-1}$).

4. DISCUSSION

The 3.4σ detection of the radial-velocity variation induced by WASP-47e further diminishes the probability that the corresponding transit signal is an “astrophysical false positive” due to an unresolved eclipsing binary. Thus, WASP-47 is unambiguously the first known case of a hot Jupiter accompanied by a shorter-period, smaller planetary companion. The compactness and apparent flatness of the system, along with the prograde rotation of the host star (Sanchis-Ojeda et al. 2015), seem consistent with quiescent migration through the protoplanetary disk (Lin et al. 1996), as opposed to dynamically hotter scenarios involving planet-planet encounters or

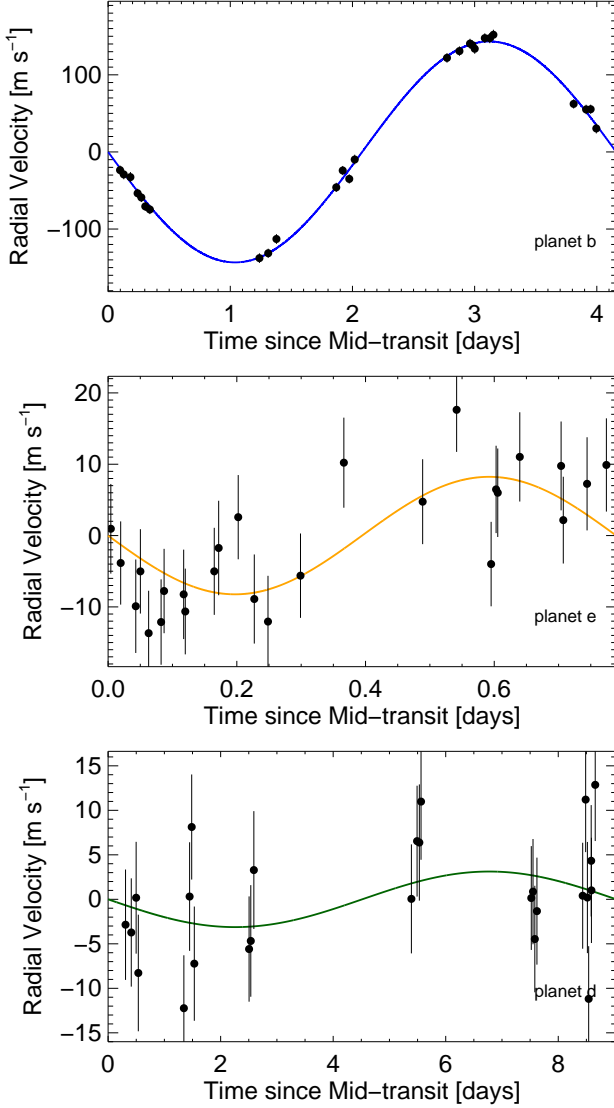


FIG. 2.— Radial velocity as a function of the orbital phase of each of the three inner planets. In each case, the modeled contributions of the other two planets has been removed, before plotting.

perturbations from distant stars. Simulations by Mustill et al. (2015) showed that high-eccentricity migration of a giant planet is often destructive to the inner planetary system.

Barring subsequent disruption, neighboring planets undergoing disk migration are likely to be trapped in first-order mean-motion resonance (MMR) (e.g. Peale 1976). It is therefore interesting that the period ratios between the inner three planets of WASP-47 are not especially close to any first-order MMR. The period ratio between the outer pair (b and d) is 2.17, which is quite typical of the period ratios for neighboring planets observed in the *Kepler* multiplanet systems (Steffen & Hwang 2015). There does not yet seem to be a convincing explanation for the prevalence of this period ratio. Furthermore, the ratio of 5.27 for the inner two planets (b and e) conforms with a trend noted by Steffen & Farr (2013): the shortest-period planets ($\lesssim 2$ days) tend to have unusually large period ratios with their closest neighbors.

With a period shorter than one day, the innermost planet e is an example of an “ultra-short period” (USP) planet, as classi-

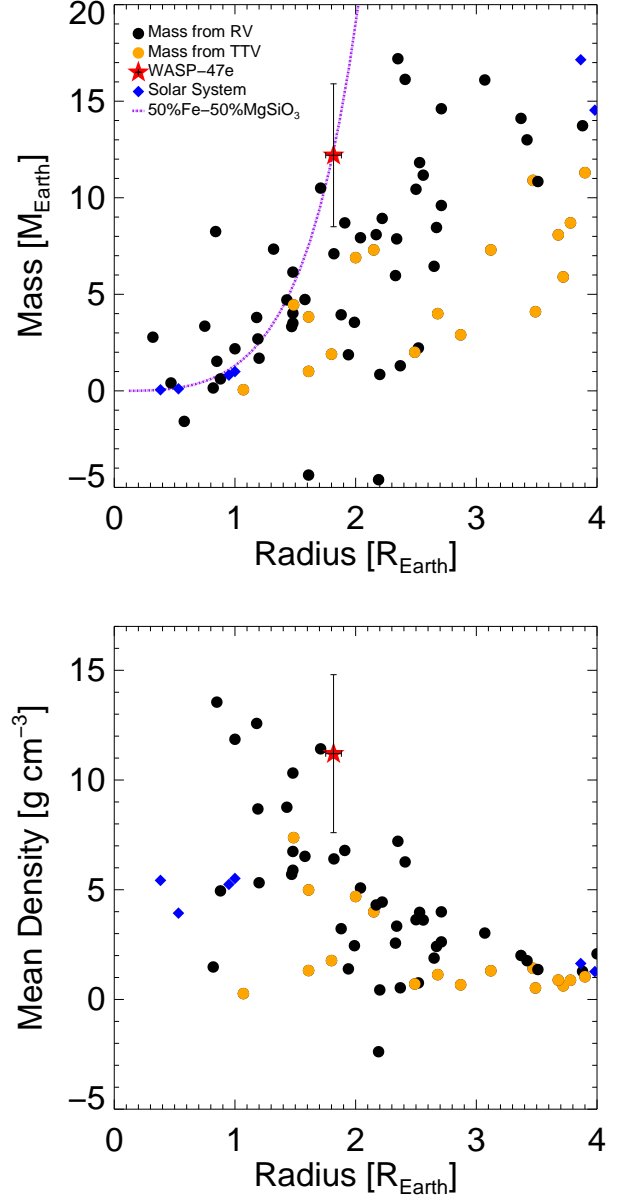


FIG. 3.— *Top.*—Masses and sizes of exoplanets (compiled by Wolfgang et al. 2015, see references therein), as measured through the Doppler method (black) and the TTV method (orange). The blue diamonds are solar system planets. The red star is WASP-47e, which lies close to the theoretical curve for a composition of 50% Fe and 50% MgSiO_3 (Zeng & Sasselov 2013) (a stony-iron composition). *Bottom.*—Mean densities and sizes of the same sample.

fied by Sanchis-Ojeda et al. (2014). Those authors found that USP planets are almost always smaller than $2 R_{\oplus}$ and frequently appear in compact multiple-planet systems, and indeed WASP-47e has both of these characteristics. Relatively few masses have been measured for USP planets. They are generally expected to be rocky, with thin or nonexistent atmospheres, because of the intense heat from the nearby star and the possibility of photoevaporation of any thick atmosphere. One notable exception is 55 Cnc e, an USP planet that does seem to have a thick atmosphere, judging from its relatively low mean density (Winn et al. 2011; Demory et al. 2011). In contrast, our mass and radius measurements for WASP-47e

imply a mean density of $11.2 \pm 3.6 \text{ g cm}^{-3}$, which is consistent with a rocky planet. For example, the measured dimensions of WASP-47e are compatible with the models of Zeng & Sasselov (2013) for a stony-iron composition (50% Fe and 50% MgSiO_3), as illustrated in Figure 3.

In fact the measured mass and density of WASP-47e are both somewhat higher than would be predicted based on the few previous measurements of planets in the same size range. The empirical mass-radius relationship of Weiss & Marcy (2014) predicts a mass for WASP-47e of $4.5 M_{\oplus}$. Likewise, the probabilistic relationship of Wolfgang et al. (2015) predicts a mass of $5.9 \pm 1.9 M_{\oplus}$, and gives a likelihood of only $\sim 3\%$ for a planet with the measured dimensions of WASP-47e. Rogers (2015) argued that $1.6 R_{\oplus}$ represents a critical radius, separating smaller planets with a mainly rocky composition from larger planets with substantial low-density atmospheres. WASP-47e with its radius of $1.8 R_{\oplus}$ and apparently rocky composition, seems to be an exception to this rule. This discrepancy may be because the planet samples analyzed by Rogers (2015) were not as strongly irradiated as WASP-47e. The strong irradiation could have stripped the planet of its volatile atmosphere, thereby leaving behind the dense rocky core. Based on current estimates of the stellar parameters and the orbital distance of WASP-47e, the planet receives roughly 3800 times more stellar radiation than the Earth. The combination of strong irradiation and large radius of WASP-47e is in agreement with the finding of Wolfgang & Lopez (2015) who showed that the inclusion of the flux dependence broadens the radius range over which the expected composition changes from rocky to volatile-enhanced. In their models, the transition ranges over $1.2\text{--}1.8 R_{\oplus}$.

It is also interesting to compare the Doppler and TTV methods for measuring the planet masses. For the giant planet, the TTV mass of $341^{+73}_{-55} M_{\oplus}$ is within about 1σ of our Doppler mass of $370 \pm 29 M_{\oplus}$. For the inner planet, the TTV analysis led to an upper limit of $22 M_{\oplus}$, which is compatible with our Doppler mass of $12.2 \pm 3.7 M_{\oplus}$. For the outer planet, the Doppler mass constraint of $10.4 \pm 8.4 M_{\oplus}$ is consistent with the TTV constraint of $15.2^{+6.7}_{-7.6} M_{\oplus}$. All these results are in accordance, although there is still plenty of scope for improving both measurements and sharpening the comparison, particu-

larly for the smaller planets.

Another intriguing feature of WASP-47 is the diversity among the properties of the inner three planets. The radius ratios, $R_b/R_e = 7.0 \pm 0.5$ and $R_b/R_c = 3.5 \pm 0.2$, are among the most extreme of neighboring planets observed by *Kepler*. Out of the 1020 neighboring pairs that appear in the NASA Exoplanet Archive catalog of Kepler Objects of Interest (KOIs), only 27 have a radius ratio larger than 3.5, and only 2 pairs have radius ratio larger than 7.0. The density contrast between b and e is 11 ± 5 , which is subject to large uncertainty but may be even higher than the density contrast of 8.4 ± 1.5 between Kepler-36b and c (Carter et al. 2012), an exemplar of the phenomenon of dissimilar neighboring planets. Curiously, the progression of the apparent compositions of planets e, b, and d, from rocky to Jovian to volatile-enhanced, matches the order we see in our much more spread-out solar system.

The discovery and confirmation of additional close planetary companions of this previously known hot Jupiter also raises the question: how many of the other known hot Jupiters have close-in companions? A picture had been developing that hot Jupiters are “lonely” in the sense of lacking close planetary companions (Steffen et al. 2012; Wright et al. 2009), but have we really excluded the possibility of small USP planets among the sample of hundreds of known hot Jupiters? It seems worthwhile to scrutinize those systems in greater detail, through ground-based photometry, space-based photometry with the *K2* and upcoming *TESS* missions (Ricker et al. 2014), and perhaps even with intensive Doppler programs.

We thank the referee for a very stimulating review of the manuscript. Work by FD and JNW was supported by the NASA Origins program (grant NNX11AG85G) as well as the *Transiting Exoplanet Survey Satellite* mission. AV is supported by the National Science Foundation Graduate Research Fellowship, Grant No. DGE 1144152. Australian access to the Magellan Telescopes was supported by the Australian Federal Government through the Department of Industry and Science.

Facilities: Magellan:Clay (Planet Finder Spectrograph)

REFERENCES

- Agol, E., Steffen, J., Sari, R., & Clarkson, W. 2005, *MNRAS*, 359, 567
- Becker, J. C., Vanderburg, A., Adams, F. C., Rappaport, S. A., & Schwengeler, H. M. 2015, *ArXiv e-prints*, arXiv:1508.02411
- Butler, R. P., Marcy, G. W., Williams, E., et al. 1996, *PASP*, 108, 500
- Carter, J. A., Agol, E., Chaplin, W. J., et al. 2012, *Science*, 337, 556
- Crane, J. D., Shethman, S. A., Butler, R. P., et al. 2010, in *Society of Photo-Optical Instrumentation Engineers (SPIE) Conference Series*, Vol. 7735, *Society of Photo-Optical Instrumentation Engineers (SPIE) Conference Series*, 53
- Demory, B.-O., Gillon, M., Deming, D., et al. 2011, *A&A*, 533, A114
- Dressing, C. D., Charbonneau, D., Dumusque, X., et al. 2015, *ApJ*, 800, 135
- Fabrycky, D. C., Lissauer, J. J., Ragozzine, D., et al. 2014, *ApJ*, 790, 146
- Goodman, J. & Weare, J., 2010, *Comm. App. Math. Comp. Sci.*, 5, 65
- Gelman, A. & Rubin, D., 1992, *Stat. Sci.*, 7, 457-472
- Hellier, C., Anderson, D. R., Collier Cameron, A., et al. 2012, *MNRAS*, 426, 739
- Holman, M., Touma, J., & Tremaine, S. 1997, *Nature*, 386, 254
- Holman, M. J., & Murray, N. W. 2005, *Science*, 307, 1288
- Howard, A. W., Sanchis-Ojeda, R., Marcy, G. W., et al. 2013, *Nature*, 503, 381
- Howell, S. B., Sobeck, C., Haas, M., et al. 2014, *PASP*, 126, 398
- Innanen, K. A., Zheng, J. Q., Mikkola, S., & Valtonen, M. J. 1997, *AJ*, 113, 1915
- Jontof-Hutter, D., Lissauer, J. J., Rowe, J. F., & Fabrycky, D. C. 2014, *ApJ*, 785, 15
- Jontof-Hutter, D., Rowe, J. F., Lissauer, J. J., Fabrycky, D. C., & Ford, E. B. 2015, *Nature*, 522, 321
- Lin, D. N. C., Bodenheimer, P., & Richardson, D. C. 1996, *Nature*, 380, 606
- Lissauer, J. J., Jontof-Hutter, D., Rowe, J. F., et al. 2013, *ApJ*, 770, 131
- Marcy, G. W., Isaacson, H., Howard, A. W., et al. 2014, *ApJS*, 210, 20
- Mazeh, T., Krymowski, Y., & Rosenfeld, G. 1997, *ApJ*, 477, L103
- Meschiari, S., Wolf, A. S., Rivera, E., et al. 2009, *PASP*, 121, 1016
- Mortier, A., Santos, N. C., Sousa, S. G., et al. 2013, *A&A*, 558, A106
- Mustill, A. J., Davies, M. B., & Johansen, A. 2015, *ApJ*, 808, 14
- Neveu-VanMalle, M., Queloz, D., Anderson, D. R., et al. 2015, *ArXiv e-prints*, arXiv:1509.07750
- Peale, S. J. 1976, *ARA&A*, 14, 215
- Pepe, F., Cameron, A. C., Latham, D. W., et al. 2013, *Nature*, 503, 377
- Rasio, F. A., & Ford, E. B. 1996, *Science*, 274, 954
- Ricker, G. R., Winn, J. N., Vanderspek, R., et al. 2014, in *Society of Photo-Optical Instrumentation Engineers (SPIE) Conference Series*, Vol. 9143, *Society of Photo-Optical Instrumentation Engineers (SPIE) Conference Series*, 20
- Rogers, L. A. 2015, *ApJ*, 801, 41
- Sanchis-Ojeda, R., Rappaport, S., Winn, J. N., et al. 2014, *ApJ*, 787, 47
- Sanchis-Ojeda, R., Winn, J. N., Dai, F., et al. 2015, *ArXiv e-prints*, arXiv:1509.05337

- Schmitt, J. R., Agol, E., Deck, K. M., et al. 2014, *ApJ*, 795, 167
- Steffen, J. H., & Farr, W. M. 2013, *ApJ*, 774, L12
- Steffen, J. H., & Hwang, J. A. 2015, *MNRAS*, 448, 1956
- Steffen, J. H., Ragozzine, D., Fabrycky, D. C., et al. 2012, *Proceedings of the National Academy of Science*, 109, 7982
- Weidenschilling, S. J., & Marzari, F. 1996, *Nature*, 384, 619
- Weiss, L. M., & Marcy, G. W. 2014, *ApJ*, 783, L6
- Winn, J. N., Matthews, J. M., Dawson, R. I., et al. 2011, *ApJ*, 737, L18
- Wolfgang, A., & Lopez, E. 2015, *ApJ*, 806, 183
- Wolfgang, A., Rogers, L. A., & Ford, E. B. 2015, *ArXiv e-prints*, arXiv:1504.07557
- Wright, J. T., Upadhyay, S., Marcy, G. W., et al. 2009, *ApJ*, 693, 1084
- Zeng, L., & Sasselov, D. 2013, *PASP*, 125, 227